Military Technical College
Kobry El-Kobbah,
Cairo, Egypt

11th International Conference
on Electrical Engineering
ICEENG 2018

Working out a Method for Choosing and Calculating the Key Parameters and Characteristics of Onboard Remote Sensing Electro-Optical Systems

H.M. El-Sheikh* and Yu.G.Yakushenkov**

ABSTRACT

Working out a method for choosing and calculating the key parameters and characteristics of the Onboard Remote Sensing Electro–Optical systems ORSEOS, where in the formulas for determination of the interconnection between the spatial from perspective distortions and the temporal, energetic and spectral resolutions of that ORSEOS for remote sensing application for a variety of scene viewing modes is offered. These dependences can be compared with the user's requirements, upon the permission values of the design parameters of the modern main units of the electro-optical system. This method may be help in selecting the operational geometrical-optical scanning scheme of the ORSEOS that mounted on the flying vehicle.

KEY WORDS

Onboard remote sensing electro-optical systems (ORSEOS), temporal resolution, spatial resolution, energetic resolution, spectral resolution, Fabry-Perot interferernce filter (FPF), operational geometrical-optical scanning scheme, perspective distortion, systematic oblique photography.

1. Introduction

Selecting the operational geometrical-optical scanning scheme of the ORSEOS that mounted on the flying vehicle depends upon the required task, which is closely associated with the spatial, temporal, spectral and energetic resolutions of that ORSEOS. Hence, it is important to match between the operational scanning scheme and the predetermined user’s requirements with the possibilities of the modern

* Egyptian Armed Forces.
** Moscow State University of Geodesy and Cartography (MIIGAiK),Moscow.

ORSEOS basic parts, first and foremost, with the parameters of optical system (lens) and focal plane array (FPA). In [1-7], some principles for selecting the ORSEOS operational scanning schemes are explained, the determination of the main design parameters and characteristics of the infrared imaging systems for remote sensing applications are discussed, and also, provide some possible ways for choosing and evaluating the ORSEOS basic parts building structure and their corresponding design parameters and characteristics.

This paper is devoted to make a relation between the spatial resolution (defined as the linear size l_x of the projected detector element onto the scene) and the temporal resolution (defined as the dwell time τ_{do} taken to scan across their corresponding spatial), also the paper makes a connection between the spatial and temporal resolutions with the spectral resolution $\Delta\lambda$ and energetic resolution (defined by noise-equivalent differential reflectance $NE\Delta\rho$ or by the noise-equivalent differential temperature $NE\Delta T_t$) and to explain the effect of the perspective distortion, arisen from the off-optical axes case rather than the oblique views operating modes, upon the ORSEOS's spatial, temporal, energetic, spectral resolutions. A brief discussion for systematic oblique photography using multiple ORSEOSs is offered. A suggested low altitude operational geometrical-optical scheme is analyzed.

The acquisition of oblique photography by the manned and unmanned flying platform is an area of strong development. There is a strong movement towards combining traditional nadir (vertical) images with oblique images acquired at high angles. Currently, the systematic oblique photography using multiple ORSEOSs is the much interest. To understand how these resolutions depends upon the operation mission parameters including, the flying velocity V_y, the flight height H and the ORSEOS look angle Ω'_x and Ω'_y; it is beneficial to examine these resolutions in the vertical, side oblique and forward oblique operational viewing modes [1-7].

2. Discussion

The generic operational geometrical-optical scheme of the ORSEOS in the vertical, side oblique and forward oblique viewing modes is illustrated in fig.(1). One of the ways to achieve this operational scheme is that, a flying vehicle 1 carries the ORSEOS 2 over the scene 5 and flies along the scene in the y direction with a velocity V_y at the object plane, while the ORSEOS, at the same time, viewing across the scene 5 in the x direction by the means of the optic-mechanical or electronic scanning with a velocity v_x (for example, by the aid of the multi-element FPA 4).

The ORSEOS views the underlying surface (scene) 5 of dimensions $L_{xo} \times L_{yo}$ from a height H via atmosphere 10 by the means of the multi-element FPA 4 of an angular size $2\Omega_x \times 2\Omega_y$ (nadir field of view FOV), where the FPA is located at the focal plane of the ORSEOS lens 3 with a focal length f'. The FPA 4 may formatted in N_x individual photosensitive elements (pixels) 6 operating in x direction, or may include a format area having $N_x \times N_y$ pixels arranged in columns and rows (lines), where N_x ***is*** the number of pixels operating in x direction and N_y is the number of pixels operating in y direction. Assuming a full FPA, 100% fill factor, the pixel pitch d_x and d_y in the x, y direction, respectively, are defining the detector active dimensions, while there is no gaps between the detector elements. The IFOV angles $\mathbf{2\omega_{xo}}$ and $\mathbf{2\omega_{yo}}$ are the angle subtended by the d_x and d_y in the x, y direction, respectively, while, the FOV angles $2\Omega_x$ and $2\Omega_y$ are the total angle subtended by the FPA size ($N_x \times d_x$) and ($N_x \times d_y$) in the x, y direction, respectively. In the vertical viewing mode 7, the ORSEOS's optical axis is perpendicular to the FPA 4 surface where the optical axis coincides on the plumb line. The FPA array 4 or the detector element (pixel) 6 is projected onto the scene 5 surface by the system optic (lens) 3 without any perspective distortion, the fundamental spatial resolution l_{xo} and l_{yo} represent the minimum linear sizes of the projected detector elements (pixels) onto the scene in the x, y direction, respectively. In the side oblique mode 8, the ORSEOS's optical axis is also perpendicular to the FPA 4 surface while it is deviated by an arbitrary look angle Ω'_x in the x direction relative to the plumb line. The values l_{xi} and l_{yi} defining the i^{th} spatial resolution in the x, y direction, respectively, of each projected pixel 11 onto the scene 5 within the FPA 4 format array. The angles θ_i representing the angles within the $2\Omega_x$ that measured to the center of each column within FPA 4 format and the signs (+,–) determining the column location with respect to the optical axis. In the forward oblique mode 9, again, the ORSEOS's optical axis is perpendicular to the FPA 4 surface but it is deviated by an arbitrary look angle Ω'_y in the y direction relative to the plumb line. The values l_{xj} and l_{yj} representing the j^{th} spatial resolution in the x, y direction, respectively, of each projected pixel 12 onto the scene 5 within the FPA 4 format array. The angles θ_j defining the angles within the $2\Omega_y$ that measured to the center of each row within FPA format and the signs (+,–) indicate the row location with respect to the optical axis.

3. Spatial Resolution

Table 1: Basic parameters and characteristics related to the requirements of the ORSEOS spatial resolution:

Item			Vertical mode $\Omega'_x = \Omega'_y = 0^o$	Side oblique mode $\Omega'_y = 0^o$, $\Omega'_x \le 90^o$	Forward oblique mode $\Omega'_x = 0^o$, $\Omega'_y \le 90^o$
Pixel distoriton cofficient	in x direction	on-axis	$k_x = k'_x = 1$	$k_x = 1/\cos^2\Omega'_x$;	$k'_x = 1/\cos\Omega'_y$;
	in y direction		$k_y = k'_y = 1$	$k_y = 1/\cos\Omega'_x$;	$k'_y = 1/\cos^2\Omega'_y$;
	in x direction	off-axis	$k_{xi} = k_{xj} = 1$	$k_{xi} = \cos^2\theta_i/\cos^2(\Omega'_x \pm \theta_i)$; $\theta_i \approx \tan^{-1}(id_x/f')$, $i=0,1,.,N_x/2$	$k_{xj} = \cos\theta_j/\cos(\Omega'_y \pm \theta_j)$; $\theta_j \approx \tan^{-1}(jd_y/f')$, $j= 0,1,.,N_y/2$
	in y direction		$k_{yi} = k_{yj} = 1$	$k_{yi} = \cos\theta_i/\cos(\Omega'_x \pm \theta_i)$; $\theta_i \approx \tan^{-1}(id_x/f')$, $i=0,1,.,N_x/2$	$k_{yj} = \cos^2\theta_j/\cos^2(\Omega'_y \pm \theta_j)$; $\theta_j \approx \tan^{-1}(jd_y/f')$, $j= 0,1,.,N_y/2$
Pixel spatial resolution in x direction		on-axis	$l_{x0} \approx d_x H / f'$	$l_x \approx l_{xo}k_x$	$l'_x \approx l_{xo}k'_x$
		off-axis		$l_{xi} \approx l_{x0}\, k_{xi}$	$l_{x\,j} \approx l_{x0}\, k_{xj}$
Pixel spatial resolution in y direction		on-axis	$l_{y0} \approx d_y H / f'$	$l_y \approx l_{yo}k_y$	$l'_y \approx l_{yo}k'_y$
		off-axis		$l_{yi} \approx l_{yo}\, k_{yi}$	$l_{y\,j} \approx l_{yo}\, k_{yj}$
Pixel projected area on the underlying surface (scene)		on-axis	$A_{\text{пп}0} \approx l_{x0}l_{y0}$	$A_{\text{пп}} \approx A_{\text{пп}0}\, k_xk_y$	$A'_{\text{пп}} \approx A_{\text{пп}0}\, k'_x k'_y$
		off-axis		$A_{\text{пп}i} \approx A_{\text{пп}0}\, k_{xi}k_{yi}$	$A'_{\text{пп}j} \approx A_{\text{пп}0}\, k_{xj}k_{yj}$
Pixel viewing angle, suptended by projected pixel on scene at the enterance aperature of a lens		on-axis	$\Omega_0 \approx D^2/4H^2$	$\Omega_{\text{вб}} \approx \Omega_0/k_x$	$\Omega'_{\text{вп}} \approx \Omega_0/k'_y$
		off-axis	$\Omega_{ij} \approx \Omega_0 \cos^3\theta_{ij}$;	$\Omega_{\text{вб}ij} \approx \Omega_0\cos^3\theta_{ij}/k_{xi}$	$\Omega'_{\text{вп}ij} \approx \Omega_0\cos^3\theta_{ij}/k_{yj}$
			$\cos\theta_{ij} \approx \cos\theta_i \cos(\tan^{-1}(\cos\theta_i \tan\theta_j))$		
FPA total coverage in x direction			$L_{x0} \approx N_x\, l_{x0}$	$L_x \approx L_{x0}\, k_x$	$L'_x \approx L_{x0}\, k'_x$
FPA total coverage in y direction			$L_{y0} \approx N_y\, l_{y0}$	$L_y \approx L_{y0}\, k_y$	$L'_y \approx L_{y0}\, k'_y$
FPA total coverage area			$A_{\text{к}0} \approx N_xN_yA_{\text{пп}0}$	$A_{\text{к}} \approx A_{\text{к}0}\, k_x k_y$	$A'_{\text{к}} \approx A_{\text{к}0}\, k'_x k'_y$

4. Temporal Resolution

Table 2: Basic parameters and characteristics related to the requirements of the ORSEOS temporal resolution:

Item		Vertical mode $\Omega'_x = \Omega'_y = 0^o$	Side oblique mode $\Omega'_y = 0^o$, $\Omega'_x \leq 90^o$	Forward oblique mode $\Omega'_x = 0^o$, $\Omega'_y \leq 90^o$
Pixel dwell time in y direction	on-axis	$T_{y0} \approx l_{y0}/V_y$	$T_y \approx T_{y0}k_y$	$T'_y \approx T_{y0}k'_y$
	off-axis		$T_{yi} \approx T_{y0}k_{yi}$	$T_{yj} \approx T_{y0}\, k_{yj}$
Pixel scanning rate in y direction	on-axis	$f_{y0} \approx 1/ T_{y0}$	$f_y \approx f_{y0} / k_y$	$f'_y \approx f_{y0} / k'_y$
	off-axis		$f_{yi} \approx f_{y0} / k_{yi}$	$f'_{yj} \approx f_{y0} /k'_{yj}$
Pixel dwell time in x direction	on-axis	$\tau_{d0} \approx T_{y0}/ N_x$	$\tau_d \approx \tau_{d0}\, k_y$	$\tau'_d \approx \tau_{d0}\, k'_y$
	off-axis		$\tau_{di} \approx \tau_{d0}\, k_{yi}$	$\tau_{dj} \approx \tau_{d0}\, k_{yj}$
Pixel scanning velocity in x direction	on-axis	$v_{x0} \approx l_{x0} /\tau_{d0}$	$v_x \approx v_{x0}\, k_y$	$v'_x \approx v_{x0}/k'_x$
	off-axis		$v_{xi} \approx v_{x0}\, k_{yi}$	$v_{xj} \approx v_{x0}/k_{xj}$
Pixel readout circuit temporal frequency	on-axis	$f_{d0} \approx 1/\tau_{d0}$	$f_d \approx f_{d0} / k_y$	$f'_d \approx f_{d0} / k'_y$
	off-axis		$f_{di} \approx f_{d0} / k_{yi}$	$f_{dj} \approx f_{d0} /k_{yj}$
Pixel readout circuit electrical bandwidth	on-axis	$\Delta f_0 \approx 1/k_{\Delta f}\tau_{d0}$	$\Delta f \approx \Delta f_0/ k_y$	$\Delta f' \approx \Delta f_0/k'_y$
	off-axis		$\Delta f_i \approx \Delta f_0/ k_{yi}$	$\Delta f_j \approx \Delta f_0/ k_{yj}$
Frame to frame time		$T_{\text{к}0} \approx (N_y(1\text{-}OL_y)/\eta_{\text{к}})\, T_{y0}$	$T_{\text{к}} \approx T_{\text{к}0}\, k_y$	$T_{\text{к}} \approx T_{\text{к}0}k'_y$

Frame rate	$f_{к0} \approx 1/\ T_{к0}$	$f_к =\ f_{к0}\ /\ k_y$	$f'_к =\ f_{к0}\ /\ k'_y$

5. Spectral Resolution

Spectral resolution of the ORSEOS depends on the number of wide/narrow/selective spectral bands (windows) used to collect the information from the underlying surface (scene). Adaptive optical filters with tunable spectral characteristics may be used to apply the required spectral resolution. For example, Fabry-Perot interference filter (FPF) in matrix format $N_x \times N_y$, that may be used in a combination with FPA has the same matrix format [1-7].

The value of the spectral band of FPF for on/off-axis can be determined by [1-7].

$$\Delta\lambda_{ij} = \lambda_{2ij} - \lambda_{1ij} \approx k_{\lambda ij}\Delta\lambda, \quad k_{\lambda ij} \approx (1-(n_i/n_{eff})^2 \sin^2\theta_{ij})^{0.5}, \quad \Delta\lambda = \lambda_2 - \lambda_1 \approx \lambda_0 (1-\Re)/(\pi\Re^{0.5}),$$
$$\lambda_0 = 2\lambda_1\lambda_2/(\lambda_1+\lambda_2) = 2n_{eff}d, \qquad \lambda_{0ij} \approx k_{\lambda ij}\lambda_0, \qquad \lambda_{2ij} \approx k_{\lambda ij}\lambda_2, \qquad \lambda_{1ij} \approx k_{\lambda ij}\lambda,$$

Where $\boldsymbol{\lambda_{2ij}}$ and $\boldsymbol{\lambda_{1ij}}$ – upper and lower cutting wavelengths that related to the incident angle ($\theta_{ij} \neq 0$), n_i and n_{eff} – the index of refraction of the air and the filter material, $\boldsymbol{k_{\lambda ij}}$ – coefficient that indicate the effect of incident angles θ_{ij} upon the FPF spectral bandwidth $\Delta\lambda_{ij}$, $\Delta\lambda$ - FPF spectral bandwidth for normal incidence of the rays ($\theta_{ij} = 0$), $\boldsymbol{\lambda_2}$ and $\boldsymbol{\lambda_1}$ - upper and lower marginal wavelengths for ($\theta_{ij} = 0$), $\boldsymbol{\Re}$ - FPF Fresnel reflection coefficient, λ_0 – central wavelength for ($\theta_{ij}=0$), d – thickness of the interference filter. If the bundle of rays is inclined then the wavelengths $\boldsymbol{\lambda_0}$**,** λ_2 and $\boldsymbol{\lambda_1}$ will be drift to thwe wavelengths $\boldsymbol{\lambda_{0ij}}$**,** $\boldsymbol{\lambda_{2ij}}$ and $\boldsymbol{\lambda_{1ij}}$**.**

The value of the FPF spectral transmittance for $\theta_{ij} \neq 0$ within the working spectral band $\Delta\lambda_{ij}$ will be equal [1-7].

$$\tau_{F_{ij}} \approx \tau_{F_0} k_{F_{ij}}, \ \tau_{F0} = (1-A/(1-\Re))^2, \ k_{F_{ij}} \approx [\mathbf{1} + (\mathbf{4}\Re/(\mathbf{1}-\Re)^{\mathbf{2}})\ \mathbf{sin^2}(\pi k_{\lambda_{ij}}^2)^{0,5})]^{-1}$$

where τ_{F0} and $k_{F_{ij}}$- FPF spectral transmittance for nadir and cofficient, indicate the effect of the incident angles θ_{ij} upon the FPF spectral transmittance $\boldsymbol{\tau_{Fij}}$**,** and A – FPF absorption coefficient.

Table 3: Basic parameters related to the requirements of the ORSEOS spectral resolution (using Fabry-Perot interference filter FPF):

Item		Vertical mode $\Omega'_x = \Omega'_y = 0^o$	Side oblique mode $\Omega'_y = 0^o$, $\Omega'_x \leq 90^o$	Forward oblique mode $\Omega'_x = 0^o$, $\Omega'_y \leq 90^o$
Pixel central wavelength	on-axis	$\lambda_0 = 2\lambda_1\lambda_2/(\lambda_1+\lambda_2) = 2n_{eff}d$		
	off-axis	$\lambda_{0ij} \approx k_{\lambda ij}\lambda_0$		
Pixel upper and lower cutting wavelengths	on-axis	$\lambda_2 \approx \lambda_0 (1-\Re)/(\pi\Re^{0.5})+\lambda_1, \quad \lambda_1 \approx \lambda_2-\lambda_0 (1-\Re)/(\pi\Re^{0.5})$		
	off-axis	$\lambda_{2ij} \approx k_{\lambda ij}\lambda_2, \qquad \lambda_{1ij} \approx k_{\lambda ij}\lambda,$		
Pixel operating spectral bandwidth	on-axis	$\Delta\lambda = \lambda_2-\lambda_1 \approx \lambda_0 (1-\Re)/(\pi\Re^{0.5})$		
	off-axis	$\Delta\lambda_{ij} = \lambda_{2ij}-\lambda_{1ij} \approx k_{\lambda ij}\Delta\lambda, \ \boldsymbol{k_{\lambda ij}} \approx (1-(n_i/n_{eff})^2\sin^2\theta_{ij})^{0.5}$		
Pixel spectral transmittance	on-axis	$\tau_{F0} = (1-A/(1-\Re))^2$		
	off-axis	$\tau_{F_{ij}} \approx \tau_{F_0} k_{F_{ij}}, \ k_{F_{ij}} \approx [\mathbf{1} + (\mathbf{4}\Re/(\mathbf{1}-\Re)^{\mathbf{2}})\ \mathbf{sin^2}(\pi k_{\lambda_{ij}}^2)^{0,5})]^{-1}$		

6. Energetic Resolution

Energetic resolution of the ORSEOS can be determined by the calculating the values of the Noise Equivelent Reflectance or Emissivty Difference $NE\Delta\rho$ or $NE\Delta\varepsilon$, and also by calculating the values of the Noise Equivilant Temperature Difference $NE\Delta T_{эс}$ (*NETD*) of the detected objects (individual parts of scene сцены, corresponding to the projection of FPA's pixels $l_x\times l_y$ at the underlying surface) within the predetermined operating spectral band [1-7].

The coefficients k_{aij}, k_{saij} and k'_{aij} that consider the changes in distances traversed by flux for different angles Ω'_x, Ω'_y and θ_{ij} should be inserted in the well-known formulas for calculating flux or illuminance/irradiance at the entrance aperature. For $\theta_{ij}\neq 0$, the coefficients $k_{c\Delta\lambda ij}$, $k_{эс\Delta\lambda ij}$ and $k_{\Delta\lambda ij}$ that determine the change in the amount of the received flux by each ^{ij}th pixel should be considered in the aforementioned formulas [1-7].

Figure 2 shows a scheme for calculating the energetic resolution of individual sections of the scene, taken for Lambertian radiators with dimensions $l_{x0}\times l_{y0}$ on the terrain, where σ_c and θ are the zenith angle of the Sun 13 and the direction of viewing the scene by a separate FPA's pixel, respectively.

In the vertical viewing mode, $\Omega'_x = \Omega'_y = 0$, the brightness (luminance & radiance) L_0 of the scene element observed in nadir, and the brightness L_{ij} of other surface elements in the wavelength band corresponding to the spectral resolution of the ORSEOS for the ij^{th} pixel will be [1-7].

$$L_0 \approx L_{c0} + L_{эс0} \qquad , \qquad L_{ij} \approx L_{cij} + L_{эсij},$$

$$L_{c0} \approx \tau_0\,(\rho/\pi)\,(r_c/r_{зс})^2\tau_1\,(\cos\sigma_c)\int_{\Delta\lambda} c_1\lambda^{-5}(e^{c2/\lambda Tc}-1)^{-1}d\lambda,$$

$$L_{эс0} \approx \tau_0\,(\varepsilon/\pi)\int_{\Delta\lambda} c_1\lambda^{-5}\,(e^{\,c2/\lambda Tэс}-1)^{-1}\,d\lambda,$$

$$L_{cij} \approx k_{aij}\tau_0(\rho/\pi)\,(r_c/r_{зс})^2\tau_1\,(\cos\sigma_c)\,k_{c\Delta\lambda ij}\int_{\Delta\lambda} c_1\lambda^{-5}(e^{c2/\lambda Tc}-1)^{-1}d\lambda \approx k_{aij}k_{c\Delta\lambda ij}L_{c0},$$

$$L_{эсij} \approx k_{aij}k_{эс\Delta\lambda ij}\,(\varepsilon/\pi)\int_{\Delta\lambda} c_1\lambda^{-5}\,(e^{\,c2/\lambda Tэс}-1)^{-1}\,d\lambda \approx k_{aij}k_{эс\Delta\lambda ij}\,L_{эс0},$$

Therefore,
$$L_{ij} \approx k_{aij}(k_{c\Delta\lambda ij}L_{c0} + k_{эс\Delta\lambda ij}\,L_{эс0}) \approx L_0\,k_{\Delta\lambda ij}k_{aij}.$$

Where $r_{зс}$ is the average distance from the scene to the Sun during the operation of the ORSEOS, r_c is the average radius of the Sun, c_1 and c_2 are Planck's law constants, T_c is the solar temperature, $T_{эс}$ is the temperature of the scene element, ε is the emissivity of the scene element, ($\rho=1-\varepsilon$) is the reflection coefficient of the scene element. $\tau_1 \approx e^{-\beta ext H_a \sec\sigma c}$ is the transmittance of the atmosphere along the path ($H_a\sec\sigma_c$) from the Sun to the scene element, H_a is the thickness of the atmosphere $k_{aij} \approx e^{-\beta ext H\,(\sec\theta ij-1)}$ is a coefficient that takes into account the variable pass length ($H\sec\theta_{ij}$) from the scene element to the ORSEOS for various angles θ_{ij}, $\tau_0 \approx e^{-\beta ext H}$ is the atmospheric transmittance in nadir observation, H is the flight altitude and ($k_{c\Delta\lambda ij}$, $k_{эс\Delta\lambda ij}$ and $k_{\Delta\lambda ij}$) are coefficients that take into account the influence of the change in the size of $\Delta\lambda_{ij}$ upon the brightness L_{cij}, $L_{эсij}$ and L_{ij}, correspondingly, which are equal to

$$k_{c\Delta\lambda ij} \approx \int_{\Delta\lambda ij} c_1\lambda^{-5}(e^{\,c2/\lambda Tc}-1)^{-1}\,d\lambda) \,/ \int_{\Delta\lambda} c_1\lambda^{-5}(e^{\,c2/\lambda Tc}-1)^{-1}\,d\lambda,$$

$$k_{эс\Delta\lambda ij} \approx \int_{\Delta\lambda ij} c_1 \lambda^{-5}(e^{\,c_2/\lambda T_{эс}}-1)^{-1}\, d\lambda) \,/ \int_{\Delta\lambda} c_1 \lambda^{-5}(e^{\,c_2/\lambda T_{эс}}-1)^{-1}\, d\lambda,$$

$$k_{\Delta\lambda ij} \approx (k_{c\Delta\lambda ij} L_{c0} + k_{эс\Delta\lambda ij}\, L_{эс0})/L_0.$$

Table 4: Basic parameters and characteristics related to the requirements of the ORSEOS energetic resolution (using Fabry-Perot interference filter FPF):

<table>
<tr><th colspan="2">Item</th><th>Vertical mode
$\Omega'_x = \Omega'_y = 0^o$</th><th>Side oblique mode
$\Omega'_y = 0^o$, $\Omega'_x \leq 90^o$</th><th>Forward oblique mode
$\Omega'_x = 0^o$, $\Omega'_y \leq 90^o$</th></tr>
<tr><td rowspan="2">Coefficient that takes into account the variable path length to the lens</td><td>on-axis</td><td>$k_a = \ k'_a = 1$</td><td>$k_a \approx \tau_0^{(ky-1)}$</td><td>$k'_a \approx \tau_0^{(k'x-1)}$</td></tr>
<tr><td>off-axis</td><td>$k_{aij} \approx \tau_0^{(\sec\theta ij-1)}$, $\tau_0 = e^{-\beta ext H}$</td><td>$k_{saij} \approx \tau_0^{(kyi\sec\theta ij-1)}$</td><td>$k'_{aij} \approx \tau_0^{(kxj\sec\theta ij-1)}$</td></tr>
<tr><td rowspan="2">Coefficient that takes into account the effect of the various values of angles θ_{ij} on τ_{Fij}</td><td>on-axis</td><td colspan="3">$k_{F_{ij}} \approx 1.$</td></tr>
<tr><td>off-axis</td><td colspan="3">$k_{F_{ij}} \approx [\,1 + (4\Re/(1-\Re)^2)\,\sin^2(\pi(1-\ (n_i/n_{eff})^2\sin^2\theta_{ij})^{0.5})]^{-1}$</td></tr>
<tr><td rowspan="3">Brightness of the scene element</td><td>on-axis</td><td>$L_0 \approx L_{c0} + L_{\text{эс}0}$
$\approx \tau_0\,[(\rho/\pi)\,(r_c/r'_{es})^2\tau_1 \cos\sigma_c$
$\times \int_{\Delta\lambda} c_1\lambda^{-5}(e^{c2/\lambda Tc} - 1)^{-1}\,d\lambda$
$+(\varepsilon/\pi)\int_{\Delta\lambda} c_1\lambda^{-5}(e^{c2/\lambda T\text{эс}} - 1)^{-1}\,d\lambda]$</td><td>$L \approx L_0\,k_a$;
$\tau_1 = e^{-\beta ext\,Ha\sec\sigma c}$</td><td>$L' \approx L_0\,k'_a$</td></tr>
<tr><td>off-axis</td><td>$L_{ij} \approx k_{aij}\,(k_{c\Delta\lambda ij}L_{c0} + k_{\text{эс}\Delta\lambda ij}\,L_{\text{эс}0})$
$\approx L_0\,k_{\Delta\lambda ij}\,k_{aij}$</td><td>$L_{sij} \approx L_0 k_{\Delta\lambda ij}\,k_{saij}$</td><td>$L'_{ij} \approx L_0 k_{\Delta\lambda ij}\,k'_{aij}$</td></tr>
<tr><td colspan="4">Coefficients that take into account the effect of changing the value of the working spectral band of the PFP $\Delta\lambda_{ij}$ in case that, the bundle of rays is incident inclined (off- axis $\theta_{ij} \neq 0$) upon the brightness L_{ij}, L_{sij}и L'_{ij}:
$k_{\Delta\lambda ij} \approx (k_{c\Delta\lambda ij}L_{c0} + k_{\text{эс}\Delta\lambda ij}\,L_{\text{эс}0})/L_0$,
where $k_{c\Delta\lambda ij} \approx \int_{\Delta\lambda ij} c_1\lambda^{-5}(e^{c2/\lambda Tc} - 1)^{-1}\,d\lambda) / \int_{\Delta\lambda} c_1\lambda^{-5}(e^{c2/\lambda Tc} - 1)^{-1}\,d\lambda$,
$k_{\text{эс}\Delta\lambda ij} \approx \int_{\Delta\lambda ij} c_1\lambda^{-5}(e^{c2/\lambda T\text{эс}} - 1)^{-1}\,d\lambda) / \int_{\Delta\lambda} c_1\lambda^{-5}(e^{c2/\lambda T\text{эс}} - 1)^{-1}\,d\lambda$.</td></tr>
</table>

Continued Table 4

Item		Vertical mode $\Omega'_x = \Omega'_y = 0^o$	Side oblique mode $\Omega'_y = 0^o$, $\Omega'_x \le 90^o$	Forward oblique mode $\Omega'_x = 0^o$, $\Omega'_y \le 90^o$
Flux arriving at the entrance pupil of the ORSEOS	on-axis	$\Phi_0 \approx A_{\text{пп}0}\, \Omega_0\, L_0$	$\Phi \approx \Phi_0 k_a$	$\Phi' \approx \Phi_0\, k'_a$
	off-axis	$\Phi_{ij} \approx \Phi_0\; k_{\Delta\lambda ij}\, k_{aij} \cos^4\theta_{ij}$	$\Phi_{sij} \approx \Phi_0\; k_{\Delta\lambda ij}\, k_{saij} \cos^4\theta_{ij}$	$\Phi'_{ij} \approx \Phi_0\, k_{\Delta\lambda ij}\, k'_{aij} \cos^4\theta_{ij}$
Signal to Noise Ratio	on-axis	$SNR_0 \approx \tau_{opt}\, \tau_{F0}\, (D^*/(A_{\text{п}}\Delta f_0)^{0.5})\, \Phi_0$	$SNR \approx SNR_0\, k_y^{0.5}\, k_a$	$SNR' \approx SNR_0\, k'^{0.5}_y k'_a$
	off-axis	$SNR_{ij} \approx SNR_0\, k_{Fij}\, k_{\Delta\lambda ij}\, k_{aij} \cos^5\theta_{ij}$	$SNR_{sij} \approx SNR_0\, k_{Fij}\, k_{\Delta\lambda ij} \times k_{yi}^{0.5} k_{saij} \cos^5\theta_{ij}$	$SNR'_{ij} \approx SNR_0\, k_{Fij}\, k_{\Delta\lambda ij} \times k'_{aij} \cos^5\theta_{ij}$
Differential flux within the spectral range $\Delta\lambda$, corresponding to the changes of $\Delta\rho$	on-axis	$\Delta\Phi_{\rho 0} \approx \tau_0\, (\Delta\rho/\pi)\, A_{\text{пп}0}\, \Omega_0\, (r_c / r'_{\text{зс}})^2 \times \tau_1 \cos\sigma_c \int_{\Delta\lambda} c_1\, \lambda^{-5}\, (e^{c2/\lambda Tc} - 1)^{-1} d\lambda$	$\Delta\Phi_{\rho} \approx \Delta\Phi_{\rho 0}\, k_a$	$\Delta\Phi_{\rho}' \approx \Delta\Phi_{\rho 0}\, k'_a$
	off-axis	$\Delta\Phi_{\rho ij} \approx \Delta\Phi_{\rho 0}\, k_{c\Delta\lambda ij}\, k_{aij} \cos^4\theta_{ij}$	$\Delta\Phi_{\rho sij} \approx \Delta\Phi_{\rho 0}\; k_{c\Delta\lambda ij}\, k_{saij} \cos^4\theta_{ij}$	$\Delta\Phi_{\rho}'{}_{ij} \approx \Delta\Phi_{\rho 0}\, k_{c\Delta\lambda ij}\, k'_{aij} \times \cos^4\theta_{ij}$
Differential flux within the spectral range $\Delta\lambda$, corresponding to the changes of $\Delta\varepsilon$	on-axis	$\Delta\Phi_{\varepsilon 0} \approx \tau_0\, (\Delta\varepsilon/\pi)\, A_{\text{пп}0}\, \Omega_0\; (r_c / r'_{\text{зс}})^2 \times \tau_1 \cos\sigma_c \int_{\Delta\lambda} c_1\, \lambda^{-5} (e^{c2/\lambda Tc} - 1)^{-1} d\lambda$	$\Delta\Phi_{\varepsilon} \approx \Delta\Phi_{\varepsilon 0}\, k_a$	$\Delta\Phi_{\varepsilon}' \approx \Delta\Phi_{\varepsilon 0}\, k'_a$
	off-axis	$\Delta\Phi_{\varepsilon ij} \approx \Delta\Phi_{\rho 0}\; k_{c\Delta\lambda ij}\, k_{aij} \cos^4\theta_{ij}$	$\Delta\Phi_{\varepsilon sij} \approx \Delta\Phi_{\varepsilon 0}\, k_{c\Delta\lambda ij}\, k_{saij} \cos^4\theta_{ij}$	$\Delta\Phi_{\varepsilon}'{}_{ij} \approx \Delta\Phi_{\varepsilon 0}\; k_{c\Delta\lambda ij}\, k'_{aij} \times \cos^4\theta_{ij}$
Differential flux within the spectral range $\Delta\lambda$, corresponding to the changes of $\Delta T_{\text{эс}}$	on-axis	$\Delta\Phi_{T\text{эс}0} \approx \tau_0\, (\Delta T_{\text{эс}}\, \varepsilon/\pi)\, A_{\text{пп}0}\, \Omega_0\, ((hc/k)/T_{\text{эс}}^2) \times \int_{\Delta\lambda} c_1\, \lambda^{-6}\, (e^{c2/\lambda T\text{эс}} - 1)^{-1} d\lambda$	$\Delta\Phi_{T\text{эс}} \approx \Delta\Phi_{T\text{эс}0}\, k_a$	$\Delta\Phi_{T\text{эс}}' \approx \Delta\Phi_{T\text{эс}0}\, k'_a$
	off-axis	$\Delta\Phi_{T\text{эс}ij} \approx \Delta\Phi_{T\text{эс}0}\; k_{T\text{эс}\Delta\lambda ij} k_{aij} \cos^4\theta_{ij}$, $k_{T\text{эс}\Delta\lambda i j} \approx \int_{\Delta\lambda ij} c_1 \lambda^{-5} (e^{\,c2/\lambda T\text{эс}} - 1)^{-1}\, d\lambda) \times 1/\int_{\Delta\lambda} c_1 \lambda^{-5} (e^{\,c2/\lambda T\text{эс}} - 1)^{-1}\, d\lambda.$	$\Delta\Phi_{T\text{эс}sij} \approx \Delta\Phi_{T\text{эс}0} k_{T\text{эс}\Delta\lambda ij} \times k_{saij} \cos^4\theta_{ij}$	$\Delta\Phi_{T\text{эс}}'{}_{ij} \approx \Delta\Phi_{T\text{эс}0}\; k_{T\text{эс}\Delta\lambda ij} \times k'_{aij} \cos^4\theta_{ij}$

End Table 4

Item		Vertical mode $\Omega'_x = \Omega'_y = 0^{o}$	Side oblique mode $\Omega'_y = 0^{o}$, $\Omega'_x \le 90^{o}$	Forward oblique mode $\Omega'_x = 0^{o}$, $\Omega'_y \le 90^{o}$
Contast to Noise Ratio, corresponding to the change of Δ_{ρ}	on-axis	$CNR_{\rho 0} \approx \tau_{opt}\, \tau_{F0}\Delta\Phi_{\rho 0} \times (D^*/(A_{\text{п}}\Delta f_0)^{0.5})$	$CNR_{\rho} \approx CNR_{\rho 0} k_y^{0.5}\, k_a$	$CNR_{\rho}' \approx CNR_{\rho 0} k'_y{}^{0.5}\, k'_a$
	off-axis	$CNR_{\rho ij} \approx CNR_{\rho 0} k_{Fij} k_{\text{с}\Delta\lambda ij} \times k_{aij}\cos^5\theta_{ij}$	$CNR_{\rho sij} \approx CNR_{\rho 0} k_{Fij} k_{\text{с}\Delta\lambda ij} \times k_{yi}^{0.5} k_{saij}\cos^5\theta_{ij}$	$CNR_{\rho}'{}_{ij} \approx CNR_{\rho 0} k_{Fij} k_{\text{с}\Delta\lambda ij} \times k_{yj}^{0.5} k'_{aij}\cos^5\theta_{ij}$
Contast to Noise Ratio, corresponding to the change of Δ_{ε}	on-axis	$CNR_{\varepsilon 0} \approx \tau_{opt}\, \tau_{F0}\Delta\Phi_{\varepsilon 0} \times (D^*/(A_{\text{п}}\Delta f_0)^{0.5})$	$CNR_{\varepsilon} \approx CNR_{\varepsilon 0} k_y^{0.5}\, k_a$	$CNR_{\varepsilon}' \approx CNR_{\varepsilon 0} k'_y{}^{0.5}\, k'_a$
	off-axis	$CNR_{\varepsilon ij} \approx CNR_{\varepsilon 0} k_{Fij} k_{\text{с}\Delta\lambda ij} \times k_{aij}\cos^5\theta_{ij}$	$CNR_{\varepsilon sij} \approx CNR_{\varepsilon 0} k_{Fij} k_{\text{с}\Delta\lambda ij} \times k_{yi}^{0.5} k_{saij}\cos^5\theta_{ij}$	$CNR_{\varepsilon}'{}_{ij} \approx CNR_{\varepsilon 0} k_{Fij} k_{\text{с}\Delta\lambda ij} \times k_{yj}^{0.5} k'_{aij}\cos^5\theta_{ij}$
Contast to Noise Ratio, corresponding to the change of $\Delta T_{\text{эс}}$	on-axis	$CNR_{T\text{эс}0} \approx \tau_{opt}\tau_{F0}\Delta\Phi_{T\text{эс}0} \times (D^*/(A_{\text{п}}\, \Delta f_0)^{0.5})$	$CNR_{T\text{эс}} \approx CNR_{T\text{эс}0} k_y^{0.5} k_a$	$CNR_{T\text{эс}}' \approx CNR_{T\text{эс}0}\, k'_y{}^{0.5}\, k'_a$
	off-axis	$CNR_{T\text{эс}ij} \approx CNR_{T\text{эс}0} k_{Fij}\, k_{T\text{эс}\Delta\lambda ij} \times k_{aij}\cos^5\theta_{ij}$	$CNR_{T\text{эс}sij} \approx CNR_{T\text{эс}0}\, k_{Fij} k_{T\text{эс}\Delta\lambda ij} \times k_{yi}^{0.5}\, k_{saij}\cos^5\theta_{ij}$	$CNR_{T\text{эс}}'{}_{ij} \approx CNR_{T\text{эс}0}\, k_{Fij}\, k_{T\text{эс}\Delta\lambda ij} \times k_{yj}^{0.5}\, k'_{aij}\, \cos^5\theta_{ij}$
Noise Equivalent Reflectivity Difference	on-axis	$NE\Delta\rho_0 \approx \Delta\rho\, /\, CNR_{\rho 0}$	$NE\Delta\rho \approx NE\Delta\rho_0\, /(k_y^{0.5}\, k_a)$	$NE\Delta\rho' \approx NE\Delta\rho_0\, /(k'_y{}^{0.5}\, k'_a)$
	off-axis	$NE\Delta\rho_{ij} \approx (NE\Delta\rho_0/k_{Fij}k_{\text{с}\Delta\lambda ij}) \times 1/(k_{aij}\cos^5\theta_{ij})$	$NE\Delta\rho_{sij} \approx (NE\Delta\rho_0/k_{Fij}k_{\text{с}\Delta\lambda ij}) \times 1/(k_{yi}^{0.5}k_{saij}\cos^5\theta_{ij})$	$NE\Delta\rho'_{ij} \approx (NE\Delta\rho_0/k_{Fij}\, k_{\text{с}\Delta\lambda ij}) \times 1/(k_{yj}^{0.5}k'_{aij}\cos^5\theta_{ij})$
Noise Equivalent Emissivity Difference	on-axis	$NE\Delta\varepsilon_0 \approx \Delta\varepsilon\, /\, CNR_{\varepsilon 0}$	$NE\Delta\varepsilon \approx NE\Delta\varepsilon_0\, /(k_y^{0.5}\, k_a)$	$NE\Delta\varepsilon' \approx NE\Delta\varepsilon_0\, /(k'_y{}^{0.5}\, k'_a)$
	off-axis	$NE\Delta\varepsilon_{ij} \approx (NE\Delta\varepsilon_0/k_{Fij}k_{\text{с}\Delta\lambda ij}) \times 1/(k_{aij}\cos^5\theta_{ij})$	$NE\Delta\varepsilon_{sij} \approx (NE\Delta\varepsilon_0/k_{Fij}\, k_{\text{с}\Delta\lambda ij}) \times 1/(k_{yi}^{0.5}k_{saij}\cos^5\theta_{ij})$	$NE\Delta\varepsilon'_{ij} \approx (NE\Delta\varepsilon_0/\, k_{Fij}\, k_{\text{с}\Delta\lambda ij}) \times 1/(k_{yj}^{0.5}k'_{aij}\cos^5\theta_{ij})$
Noise Equivalent Temperature Difference	on-axis	$NE\Delta T_{\text{эс}0} \approx \Delta T_{\text{эс}}\, /CNR_{T\text{эс}0}$	$NE\Delta T_{\text{эс}} \approx NE\Delta T_{\text{эс}0}\, /(k_y^{0.5}\, k_a)$	$NE\Delta T_{\text{эс}}' \approx NE\Delta T_{\text{эс}0}/(k'_y{}^{0.5}\, k'_a)$
	off-axis	$NE\Delta T_{\text{эс}ij} \approx (NE\Delta T_{\text{эс}0}/k_{Fij}k_{T\text{эс}\Delta\lambda ij}) \times 1/(k_{aij}\cos^5\theta_{ij})$	$NE\Delta T_{\text{эс}sij} \approx (NE\Delta T_{\text{эс}0}/k_{Fij}k_{T\text{эс}\Delta\lambda ij}) \times 1/(k_{yi}^{0.5}k_{saij}\cos^5\theta_{ij})$	$NE\Delta T_{\text{эс}}'{}_{ij} \approx (NE\Delta T_{\text{эс}0}/k_{Fij}k_{T\text{эс}\Delta\lambda ij}) \times 1/(k_{yj}^{0.5}k'_{aij}\cos^5\theta_{ij})$

7. Conclusion

- The above dependences for the selection and calculation of the main parameters and characteristics of the ORSEOS preliminary data acquisition (ORSEOS-PDA), based on the comparison of the "external" parameters and characteristics specified by the customer and the consumer of the equipment, and "internal" parameters chosen or calculated by the developer and conditioned by the existing element base of modern optical systems, optical filter and FPA, allow to calculate the resolution of these systems. In another words. If it is not possible to view the entire given scene with a high spatial resolution, it is possible to apply the geometric-optic scheme of the ORSEOS with two or more optical channels opertating in different viewing modes.

- The formulas and tables given in the paper allow us to determine the increase in the size of the projection of FPA pixels on the terrain (spatial resolution) considering the perspective distortions due to different inclination angles of the ORSEOS axis (Ω'_x, Ω'_y) and the ORSEOS internal viewing angles θ_{ij}, as well as their corresponding change in the temporal, spectral and energetic resolution values. The proposed methods allows to calculate the numerical parameters and characteristics of the ORSEOS based on the state of the modern and promising main parts (lenses, optical filter and FPA) to meet customer requirements for system resolution. The driven formulas allow estimating the ORSEOS resolutions values for each individual sections of the scene due to the projection of the FPA pixels on the underlying surface. The aforementioned development method can be used in the design of the multi/hyper spectral ORSEOS.

Figures

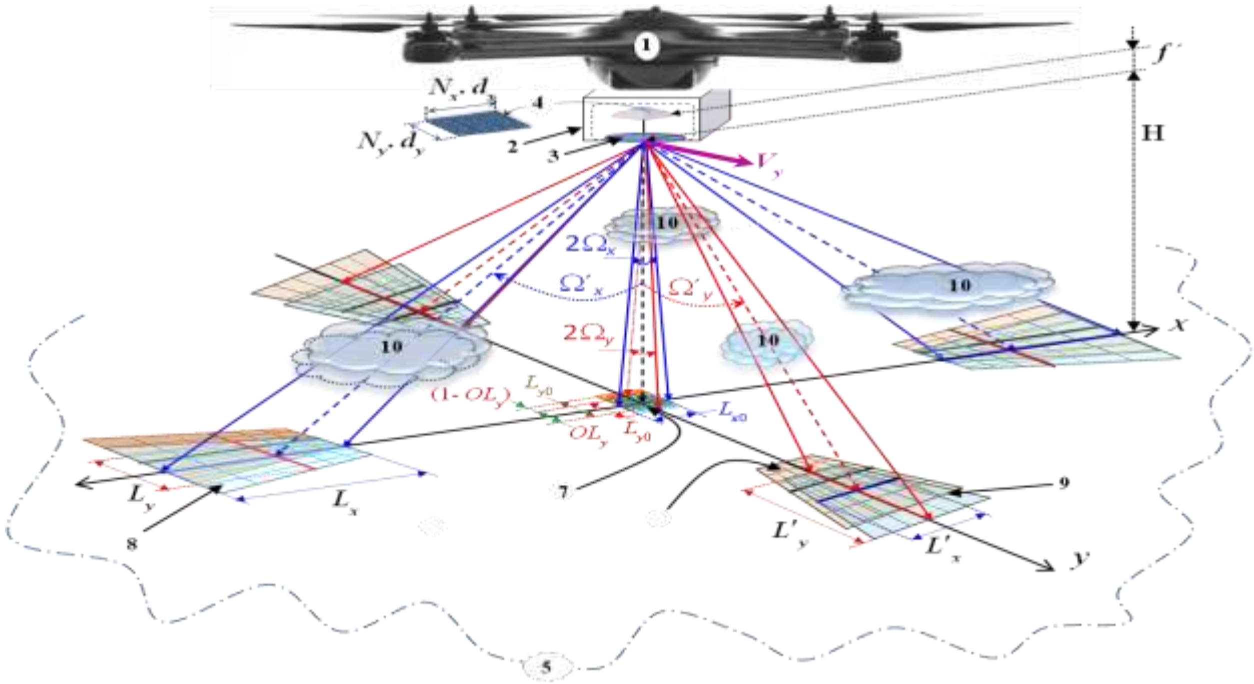

a)

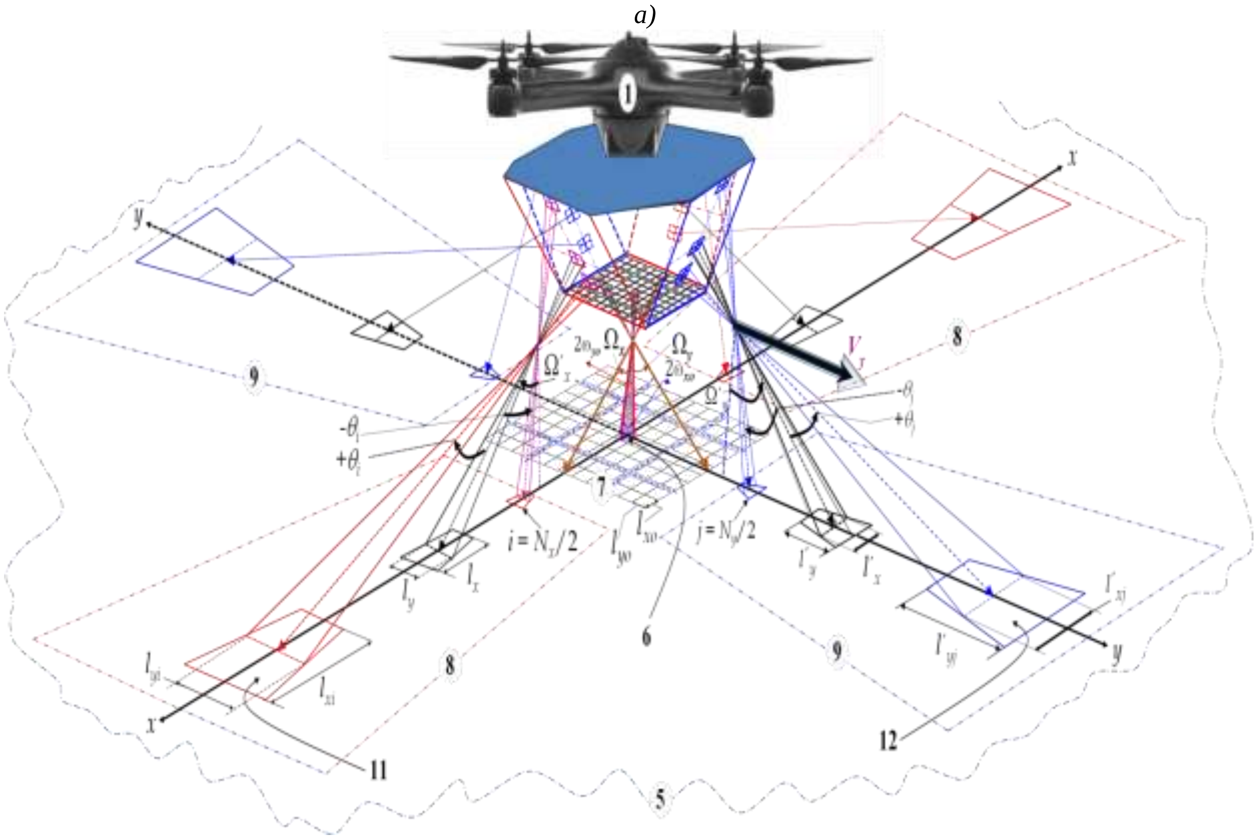

b)

Fig. 1: Generic operational geometrical-optical scheme of the ORSEOS, working a passive mode of operation.
a) step frame using one optical channel

b) step frame using two or more optical channels

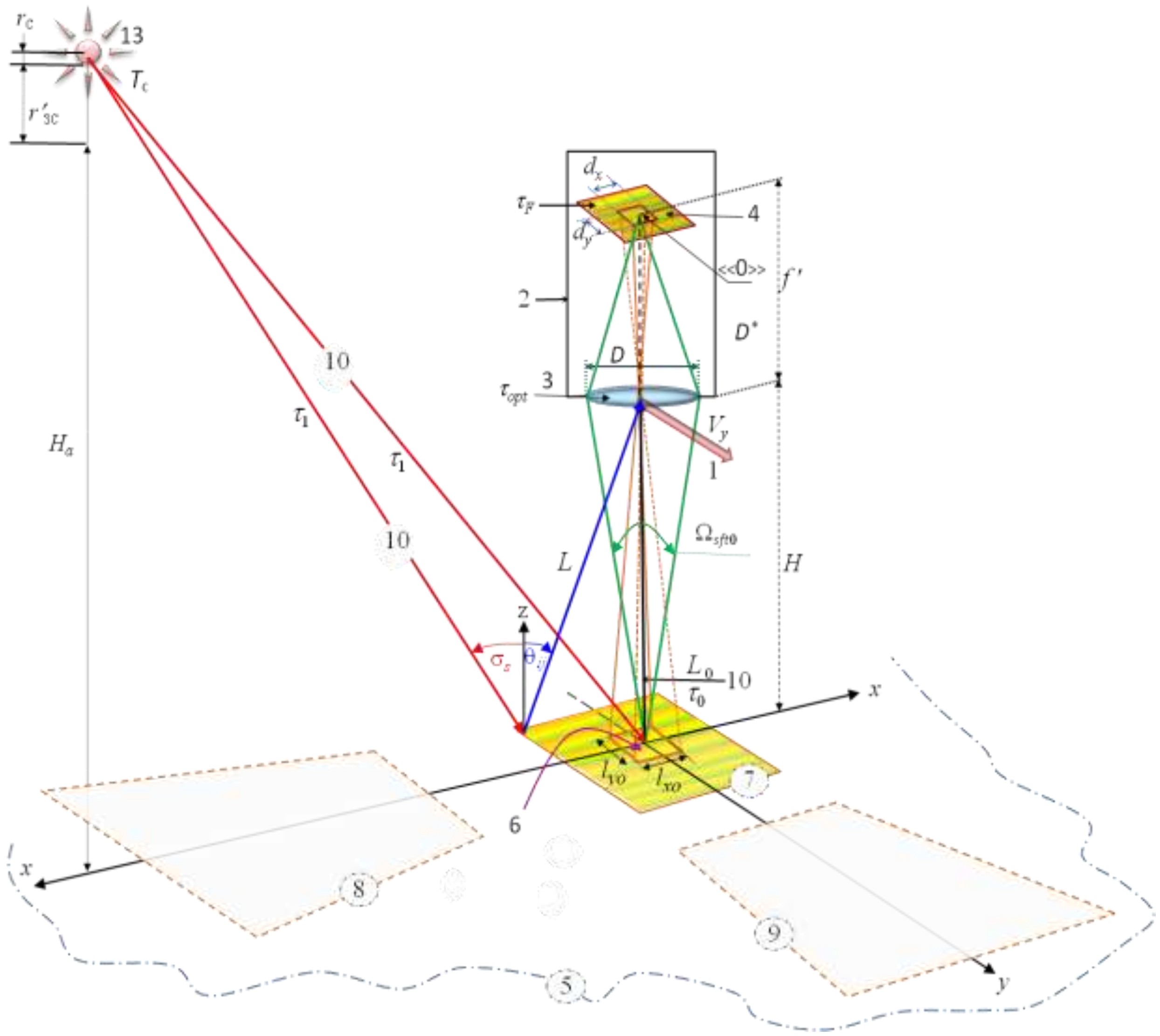

Fig. 2: Energetic resolution calculation of the ORSEOS working in a passive mode of operation.

References

1. Y.G. Yakushenkov. Choosing the scanning scheme and determination of the design parameters of remote sensing infrared systems. Journal. Izvestiya Vuzov. Geodesy and aerophotography. 2012.- № 6. - P. 118-122.
2. H.M. ElSheikh, Y.G. Yakushenkov. Spatial resolution of the onboard remote sensing electro-optical systems. Journal. Izvestiya Vuzov. Geodesy and aerophotography. 2014.- № 3. - P. 109-114.
3. H.M. ElSheikh, Y.G. Yakushenkov. Temporal resolution of the onboard remote sensing electro-optical systems. Journal. Optical information technology. 2014.- № 10. - P. 603 -606.
4. H.M. ElSheikh, Y.G. Yakushenkov. Spatial and temporal resolutions pixel level performance analysis of the onboard remote sensing electro-optical systems. JEOS: RP., V.9 (2014), № 14035-6.
5. H.M. ElSheikh, Y.G. Yakushenkov. Performance evaluation of the onboard remote sensing electro-optical systems. Journal. Izvestiya Vuzov. Geodesy and aerophotography. 2015.- № 5. - P. 93 -102.
6. http://miigaik.ru/nauka/dissertacionyy_sovet/dissertats ii/20151020151356-6539.pdf.
7. H.M. ElSheikh, Y.G. Yakushenkov. Methodology of performance error analysis evaluation of the onboard remote sensing electro-optical systems. Journal. Izvestiya Vuzov. Geodesy and aerophotography. 2016.- № 6. - P. 119 -136.